




Application of energy flow analysis in investigating machine-side oscillations of full converter-based wind generation systems

Yong Hu¹  | Siqi Bu^{1,2,3}  | Jianqiang Luo¹ 

¹ Department of Electrical Engineering, The Hong Kong Polytechnic University, Kowloon, Hong Kong S.A.R.

² Shenzhen Research Institute, The Hong Kong Polytechnic University, Shenzhen, China

³ Research Institute for Smart Energy, The Hong Kong Polytechnic University, Kowloon, Hong Kong S.A.R.

Correspondence

Siqi Bu, Department of Electrical Engineering, The Hong Kong Polytechnic University, Kowloon, Hong Kong S.A.R.

Email: siqi.bu@polyu.edu.hk

Funding information

National Natural Science Foundation of China for the Research Project, Grant/Award Number: 51807171; Guangdong Science and Technology Department for the Research Project, Grant/Award Number: 2019A1515011226; Hong Kong Research Grant Council for the Research Projects, Grant/Award Numbers: 15200418, 15219619; Department of Electrical Engineering, The Hong Kong Polytechnic University for the Start-up Fund Research Project, Grant/Award Number: 1-ZE68

Abstract

The machine-side oscillation (MSO) of the full converter-based wind generation (FCWG) systems is a critical threat to the reliable wind power supply. The introduction of the auxiliary resonance controller (ARC) to the machine-side converter (MSC) controls of FCWG can effectively improve the converter-driven stability of the power grid, but it would also complicate MSOs of FCWG. Thus, it is of great significance to study the damping feature of MSOs of FCWG. In this paper, the energy flow analysis (EFA) is applied to quantitatively investigate MSOs of FCWG. Firstly, the configuration and machine-side control loops of FCWG are briefly introduced. Then, a mode screening-based EFA is proposed for evaluating the damping feature of MSOs of FCWG in the time domain by applying the principle of the Laplace transform. After that, the eigenvalue analysis is conducted for MSOs of FCWG in the frequency domain to lay a foundation for revealing the essence of EFA. On this basis, the consistency of EFA with the eigenvalue analysis is strictly proved based on the Parseval's Theorem, which is applicable for arbitrary control schemes of FCWG. Finally, the proposed EFA is applied in numerically investigating multiple types of MSOs of FCWG in case studies.

1 | INTRODUCTION

The wind power is a predominant and typical renewable generation [1]. The stable operation of the wind generation system is of critical importance to the reliable wind power supply to the external power grid [2]. The full converter-based wind power generation (FCWG) is a preferable option for wind power integrations [3]. Compared with the doubly fed induction generator-based wind power generation, FCWG has a very different nature in dynamics. The permanent magnet synchronous generator (PMSG) and machine-side converter (MSC) of FCWG are decoupled by the DC-link from the external power grid and become relatively independent [4, 5]. However, the intermittence and fluctuation of the wind speed can trigger the inherent machine-side oscillation (MSO) of FCWG. The improper

parameter settings of controllers can lead to the poor damping performance of MSO [6]. The poorly damped MSO can have a severe impact on the wind power supply to the external power grid.

The converter-driven instability of the power grid caused by the large-scale integration of FCWG systems has been frequently reported and drawn increasing attention recently from both academia and industry [7]. The dynamics in the rotor of PMSG can be effectively utilised to mitigate the modal resonance between the FCWG system and weak grid and hence improve the converter-driven stability by equipping with an auxiliary resonance controller (ARC) on the machine side of FCWG [8]. However, the utilisation of ARCs can unfortunately introduce the grid-side oscillation mode to the originally dynamics-decoupled machine side of FCWG, and even cause the modal

This is an open access article under the terms of the [Creative Commons Attribution](https://creativecommons.org/licenses/by/4.0/) License, which permits use, distribution and reproduction in any medium, provided the original work is properly cited.

© 2022 The Authors. *IET Renewable Power Generation* published by John Wiley & Sons Ltd on behalf of The Institution of Engineering and Technology

resonance with the inherent MSO of FCWG, which would dramatically complicate and aggravate the machine-side dynamics of FCWG.

Based on the facts above, investigating the damping feature of multiple MSOs of FCWG becomes more important. Specifically, investigating the characteristics of MSOs of FCWG can help wind farm operators understand the condition of wind generation units to provide the reliable wind power supply and improve the converter-driven stability of the power grid, which is helpful to further increase the penetration of FCWG in the modern power systems. However, the MSO issue of FCWG is often ignored by researchers. Thus, the machine-side dynamics of FCWG with/without ARC should be comprehensively and quantitatively studied. It should be noted that the MSOs mentioned in this paper not only refer to the inherent MSOs of FCWG, but also the oscillation modes of the external power grid introduced by ARC (i.e., the non-inherent MSOs of FCWG).

The eigenvalue is a traditional index to characterise the damping and frequency feature of oscillation modes [9]. The damping performance with respect to an oscillation mode characterises the decaying rate of the oscillating power [10], which is related to the real part of the relevant eigenvalue [11]. The imaginary part of the eigenvalue indicates the oscillation angular frequency. When ARC introduces the grid-side dynamics to the MSC controls, the machine-side dynamics of FCWG are no longer independent. Thus, the calculation of relevant eigenvalues requires the dynamic modelling of the whole power systems. In practice, it is difficult for wind farm operators to obtain the detailed models and accurate parameters of all components in the external power systems. Even if the information of the full system model is available, the modelling and computational complexity can be significantly raised for the oscillatory stability studies of FCWG especially considering the large-scale power system [12]. Hence, the above-mentioned two points limit the application of the eigenvalue analysis in this work.

Unlike the eigenvalue analysis, the energy flow analysis (EFA) is an emerging method and provides a physical explanation on the damping performance of an oscillation event. In addition, EFA is a type of measurement-based method that can avoid the complex modelling of the whole power system [13]. At present, EFA is mainly used to locate the oscillation source, for example, [14]. Some key work on the quantitative analysis using EFA is given as follows. The calculation of the oscillatory energy flow is demonstrated in [15]. The authors in [16] reveal the relation between EFA and damping torque analysis. The damping torque coefficient in a wide frequency of interests is attempted to be derived using EFA in the frequency domain in [17]. In [18], the authors propose a methodology to estimate the eigenvalue based on EFA. The connection between EFA and modal analysis is attempted to be revealed in [19] on the basis of a specific model of synchronous generators. However, there are certain limitations in [15–19]. Firstly, reference [15–19] fail in revealing the fundamental relationship between EFA and eigenvalue analysis in a general way for any types of generator model and power network. Secondly, the work in [15–19] does not involve FCWG, which reduces the popularity and timeliness of the work. That is to say, the EFA-based quantitative analysis is

still limited in the oscillatory stability studies considering FCWG systems.

In view of the literature review of [1–8], it is important to assess the damping feature of multiple MSOs of FCWG, but sometimes the wind farm operators cannot access the detailed models and parameters of all system components. Therefore, there is a pressing need to develop an alternative method to investigate the damping feature of multiple MSOs of FCWG without the modelling. Thus, the main contributions of this paper are summarised as follows. In general, the damping feature of inherent and non-inherent MSOs of FCWG (including the potential modal resonance among them) is quantitatively investigated using a newly proposed EFA for the first time. Specifically, the contributions and merits are expressed as follows: (i) due to the limitation of the complex and sometimes unavailable modelling with respect to [9] and [10], a mode screening-based EFA is designed in the time domain to extract the damping feature of interested MSOs of FCWG without any modelling requirement; (ii) compared with the work in [15–19], the consistency between the mode screening-based EFA and eigenvalue analysis when studying MSOs of FCWG is proved and revealed, which is general for the arbitrary control schemes of FCWG in the multi-machine environment; and (iii) applying the mode screening-based EFA mentioned in (i) and (ii), the damping feature of multiple types of MSOs in different scenarios is quantitatively assessed for the first time.

The rest of this paper is organised as follows. The main configuration and machine-side control loops of FCWG are briefly introduced in Section 2. A mode screening-based EFA is proposed for MSOs of FCWG in the time domain in Section 3. Section 4 discusses the eigenvalue analysis for MSOs of FCWG, and the consistency between the mode screening-based EFA and eigenvalue analysis is strictly revealed for MSOs of FCWG in Section 5. Case studies are conducted in Section 6, and conclusions are given in Section 7.

2 | CONFIGURATION AND MACHINE-SIDE CONTROL LOOPS OF FCWG

The type configuration of FCWG is shown in Figure 1 [20, 21]. The main components of FCWG are as follows: (i) a PMSG; (ii) the MSC and its controllers; (iii) the DC-link, the grid-side converter (GSC) and their controllers; and (iv) the phase-locked loop (PLL), etc.

It can be seen from Figure 1 that the PMSG and MSC do not respond to the dynamics of the external power grid since they are decoupled from the external power grid by the DC-link. Since this paper focuses on MSO of FCWG, the machine-side control loops of FCWG are demonstrated in Figure 2, where s is the Laplacian operator; $P_{pm,i}(s)$ is the mechanical power of the i -th PMSG; $P_{we,i}(s)$ is the electric power of the i -th PMSG; $H_{pr,i}$ is the inertia constant of the rotor of the i -th PMSG; $\omega_{pr,i}(s)$ is the angular frequency of the stator of the i -th PMSG; $\omega_{prref,i}(s)$ is the reference angular frequency of the stator of the i -th PMSG; $K_{p-wt,i}$ is the integral time constant in the control loop of the

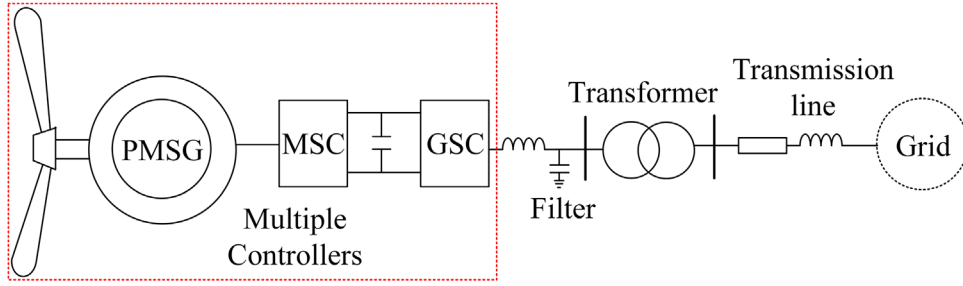


FIGURE 1 Configuration of FCWG

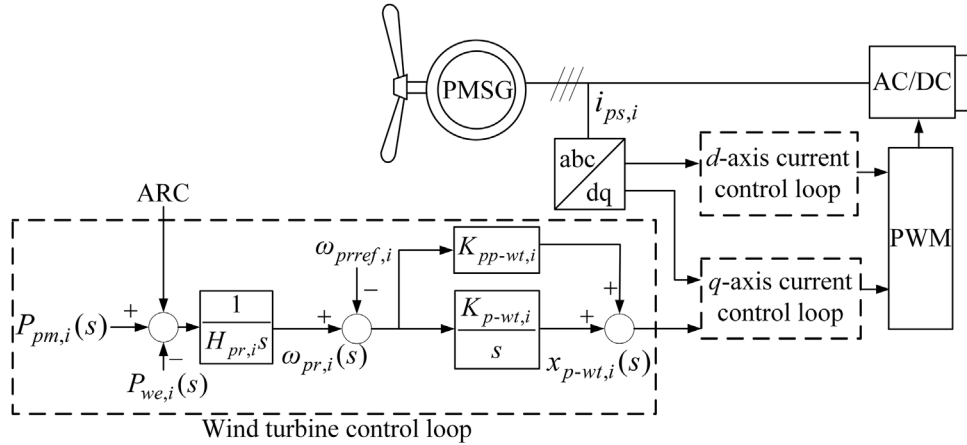


FIGURE 2 Machine-side control loops of FCWG

wind turbine of the i -th PMSG; $K_{pp-wt,i}$ is the proportional time constant in the control loop of the wind turbine of the i -th PMSG; and $x_{p-wt,i}(s)$ is an intermediate variable in the control loop of the wind turbine of the i -th PMSG. Generally, there are three control loops on the machine side of FCWG, that is, the wind turbine control loop, d -axis current control loop and q -axis current control loop. Since the discussion on EFA and its consistency with the eigenvalue analysis should be general to any control schemes, the d -axis current control loop and q -axis current control loop are represented in a general manner in Figure 2.

In the case studies, a typical scheme of d -axis current control loop and q -axis current control loop is given in Figure 3. The definition of variables in Figure 3 can be found in [8], which are not repeated here.

When there is no ARC, the machine-side dynamics are directly connected at the DC capacitor, which does not interact with the grid-side oscillation modes. That is to say, the inherent MSOs of FCWG are all independent without ARC, and their characteristics are determined by the machine-side structure as well as parameters of FCWG.

As discussed in the introduction, the rotor of PMSG can store energy and dynamics. If the FCWG is equipped with an ARC, the potential dynamic of PMSG can be utilised to improve the converter-driven stability of the power grid. On the other hand, when an ARC is installed, the grid-side oscillation mode

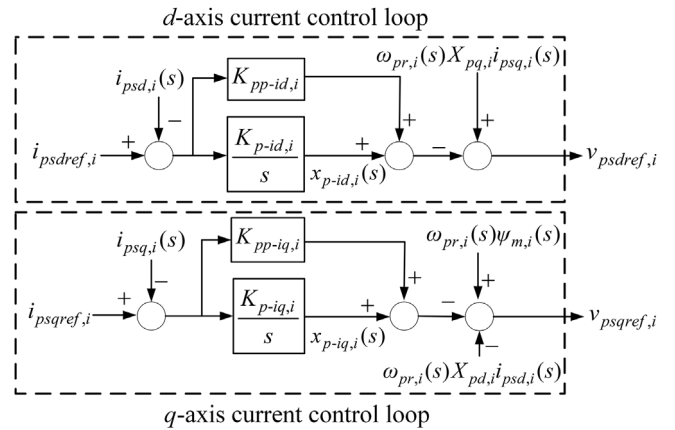


FIGURE 3 A typical control scheme of MSC

will be introduced to the machine side of FCWG, which can complicate and aggravate MSOs of FCWG. Even the modal resonance between the inherent and non-inherent MSOs can appear. Thus, the wind farm operator must pay more attention to them to ensure both the reliable wind power supply and the converter-driven stability.

The mechanism of ARC is to introduce the grid-side disturbance to the MSC controls to adjust the power output of FCWG and further to suppress the converter-driven instability.

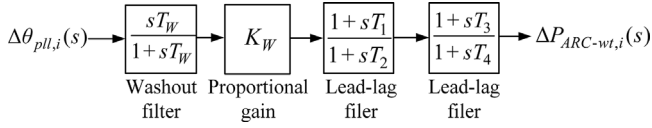


FIGURE 4 Transfer function of ARC

The transfer function of ARC is given in Figure 4, where $\Delta P_{ARC-wt,i}(s)$ is the output signal of ARC to the i -th PMSG; T_W is the time constant of the washout filter, K_W is the proportional gain, T_1 , T_2 , T_3 and T_4 are the time constants of the lead-lag filers, and $\Delta\theta_{pll,i}(s)$ is the input signal of ARC (i.e., the PLL angle variation of the i -th FCWG in the frequency domain). It can be seen that an ARC has four main parts: a washout filter, a proportional gain, and two lead-lag filters. The washout filter eliminates the DC component and select the signal with the appropriate frequency that is related to the grid-side disturbance. The proportional gain adjusts the input signal to a proper magnitude. The two lead-lag filters adjust the compensation angle to a proper one.

3 | MODE SCREENING-BASED EFA FOR MSOS OF FCWG

The typical configuration and machine-side control loops of FCWG have been given in Section 2. In this section, a mode screening-based EFA is proposed for MSOs of FCWG to extract the damping feature of the interested MSOs.

According to the definition in [17], the energy can be represented as the integral of the product of torque and speed. Based on that, the dissipation of the oscillatory energy flow of the i -th PMSG can be calculated by (1).

$$W_i^D = \int_0^{+\infty} \Delta T_{pe,i}(t) \Delta \omega_{pr,i}(t) dt \quad (1)$$

where t is the time variable; W_i^D is the dissipation of the oscillatory energy flow of the i -th PMSG; $\Delta \omega_{pr,i}(t)$ is the angular frequency deviation of the stator of the i -th PMSG in the time domain; and $\Delta T_{pe,i}(t)$ is the electric torque imbalance of the i -th PMSG.

It can be seen from (1) that the calculation of the dissipation of the oscillatory energy flow only relies on the measured signals. The electric torque imbalance can be decomposed as two components, i.e., (2).

$$\Delta T_{pe,i}(t) = K_{d,i} \Delta \omega_{pr,i}(t) + K_{s,i} \Delta \delta_{pr,i}(t) \quad (2)$$

where $K_{d,i}$ is the equivalent damping torque coefficient of the i -th PMSG; $K_{s,i}$ is the equivalent synchronous torque coefficient of the i -th PMSG; and $\Delta \delta_{pr,i}(t)$ is the power angle deviation of the i -th PMSG.

Substitute (2) into (1), and (3) can be further derived.

$$\begin{aligned} W_i^D &= \int_0^{+\infty} K_{d,i} \Delta \omega_{pr,i}^2(t) dt + \int_0^{+\infty} K_{s,i} \Delta \delta_{pr,i}(t) \Delta \omega_{pr,i}(t) dt \\ &= \int_0^{+\infty} K_{d,i} \Delta \omega_{pr,i}^2(t) dt + \frac{1}{2} K_{s,i} \left(\Delta \delta_{pr,i}^2(\infty) - \Delta \delta_{pr,i}^2(0) \right) \\ &= \int_0^{+\infty} K_{d,i} \Delta \omega_{pr,i}^2(t) dt \end{aligned} \quad (3)$$

The electric torque deviation is considered to be approximately equal to the electric power deviation for the i -th PMSG. Thus, the equivalent damping torque coefficient of the i -th PMSG can be derived as (4) with/without ARC. It is noted that $\Delta P_{ARC-wt,i}(t) = 0$ in the following two conditions: (i) there is no ARC; or (ii) ARC is installed but it does not work since there is no disturbance on the external power grid.

$$K_{d,i} = \frac{\int_0^{+\infty} (\Delta P_{we,i}(t) - \Delta P_{ARC-wt,i}(t)) \Delta \omega_{pr,i}(t) dt}{\int_0^{+\infty} \Delta \omega_{pr,i}^2(t) dt} \quad (4)$$

where $\Delta P_{we,i}(t)$ is the electric power deviation of the i -th PMSG in the time domain; and $\Delta P_{ARC-wt,i}(t)$ is the output signal of ARC to the i -th PMSG in the time domain.

For the machine side of FCWG, $K_{d,i}$ obtained by (4) is coupled with multiple MSOs and some of them may be the non-inherent MSOs introduced by ARC. That is to say, $K_{d,i}$ obtained by (4) cannot be effectively used to indicate the damping feature with respect to the interested MSO.

The definition of the Laplace transform can be expressed as (5).

$$G(s) = \int_0^{+\infty} g(t) e^{-st} dt = \int_0^{+\infty} (g(t) e^{-\sigma t}) e^{-j\omega t} dt \quad (5)$$

where $g(t)$ is a real signal; w is the imaginary part of s ; σ is the real part of s ; and $G(s)$ is the Laplace transform of $g(t)$.

On this basis, the signal $g(t)$ is reconstructed as (6).

$$g(t|\sigma) = g(t) e^{-\sigma t} \quad (6)$$

where $g(t|\sigma)$ is the reconstructed signal from $g(t)$.

It is noted that the integral interval of (5) is finite in practice. According to the Fourier series, $g(t|\sigma)$ is equivalent to the sum of a series of sub-signals with the form of (7).

$$g(t|\sigma) = \sum_{k=1}^p A_k \cos(w_k t + \alpha_k) \quad (7)$$

where p is the number of the decomposed signals; A_k is the amplitude of the k -th decomposed signal; w_k is the angular frequency of the k -th decomposed signal; and α_k is the phase angle of the k -th decomposed signal.

For an interested MSO $\lambda_d = \sigma_d \pm jw_d$, the amplitude and phase angle at w_d can be observed from the plot of the frequency-amplitude spectrum and frequency-phase spectrum of $g(t | \sigma_d)$. Thus, the decomposed sub-signal at w_d is given by (8).

$$g^{w_d}(t | \sigma_d) = A_d \cos(w_d t + \alpha_d) \quad (8)$$

where $g^{w_d}(t | \sigma_d)$ is the decomposed signal from $g(t | \sigma_d)$ with respect to w_d ; A_d is the amplitude of the decomposed signal with respect to w_d ; and α_d is the phase angle of the decomposed signal with respect to w_d .

Equation (6) is applied to reconstruct $\Delta P_{ARC-wt,i}(t)$, $\Delta P_{we,i}(t)$ and $\Delta \omega_{pr,i}(t)$ as $\Delta P_{ARC-wt,i}(t | \sigma_d)$, $\Delta P_{we,i}(t | \sigma_d)$ and $\Delta \omega_{pr,i}(t | \sigma_d)$ with respect to $\sigma = \sigma_d$. After that, (8) is further applied to decompose $\Delta P_{ARC-wt,i}(t | \sigma_d)$, $\Delta P_{we,i}(t | \sigma_d)$ and $\Delta \omega_{pr,i}(t | \sigma_d)$ as $\Delta P_{ARC-wt,i}^{w_d}(t | \sigma_d)$, $\Delta P_{we,i}^{w_d}(t | \sigma_d)$ and $\Delta \omega_{pr,i}^{w_d}(t | \sigma_d)$.

On this basis, a new concept $K_{d,i}^{\lambda_d}$ is given in (9).

$$K_{d,i}^{\lambda_d} = \frac{\int_0^{+\infty} \left(\Delta P_{we,i}^{w_d}(t | \sigma_d) - \Delta P_{ARC-wt,i}^{w_d}(t | \sigma_d) \right) \Delta \omega_{pr,i}^{w_d}(t | \sigma_d) dt}{\int_0^{+\infty} \left(\Delta \omega_{pr,i}^{w_d}(t | \sigma_d) \right)^2 dt} \quad (9)$$

where $K_{d,i}^{\lambda_d}$ is the defined damping coefficient with respect to λ_d .

4 | EIGENVALUE ANALYSIS FOR MSOS OF FCWG

In this section, the eigenvalue analysis is discussed for MSOs of FCWG to lay a foundation for revealing the essence of EFA. $\Delta \omega_{pr,i}(t)$ and $\Delta x_{p-wt,i}(t)$ are chosen as the two focused state variables. The natural damping of PMSG is ignored. According to Figure 2, the focused equations of the i -th PMSG are given as (10) and (11).

$$\frac{d\Delta \omega_{pr,i}(t)}{dt} = \frac{1}{H_{pr,i}} \left(\Delta P_{ARC-wt,i}(t) - \Delta P_{we,i}(t) \right) \quad (10)$$

$$\frac{d\Delta x_{p-wt,i}(t)}{dt} = K_{p-wt,i} \Delta \omega_{pr,i}(t) \quad (11)$$

where $\Delta x_{p-wt,i}(t)$ is the intermediate variable deviation in the control loop of the wind turbine of the i -th PMSG in the time domain. It is noted that $\Delta P_{ARC-wt,i}(t) = 0$ in the following two conditions: (i) there is no ARC; or (ii) ARC is installed but it does not work since there is no disturbance on the external power grid.

In order to represent the whole power system considering the arbitrary control schemes of FCWG in the multi-machine environment, the linearisation of the whole power system is derived as (12) considering n state variables, which is a modified state-space representation. In (12), A_{21} , A_{23} , A_{31} , A_{32} and A_{33} are the

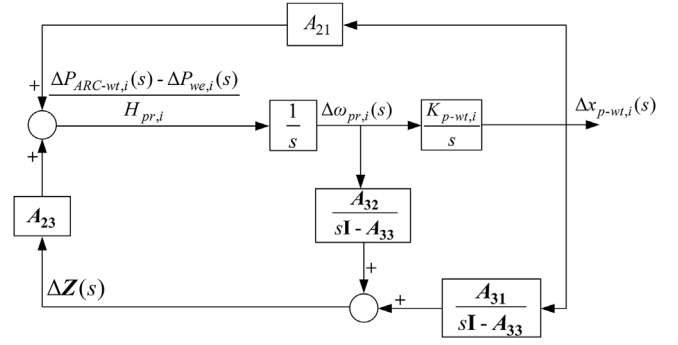


FIGURE 5 Linearised representation of an FCWG-integrated power system

blocks of the state matrix, and \mathbf{O} represents the $1 \times (n-2)$ vector in which the elements are all 0. It is noted that the dimensions of A_{23} , A_{31} , A_{32} and A_{33} are $1 \times (n-2)$, $(n-2) \times 1$, $(n-2) \times 1$ and $(n-2) \times (n-2)$, respectively.

$$\begin{bmatrix} \frac{d\Delta x_{p-wt,i}(t)}{dt} \\ \frac{d\Delta \omega_{pr,i}(t)}{dt} \\ \frac{d\Delta \mathbf{Z}(t)}{dt} \end{bmatrix} = \begin{bmatrix} 0 & K_{p-wt,i} & \mathbf{O} \\ A_{21} & 0 & A_{23} \\ A_{31} & A_{32} & A_{33} \end{bmatrix} \begin{bmatrix} \Delta x_{p-wt,i}(t) \\ \Delta \omega_{pr,i}(t) \\ \Delta \mathbf{Z}(t) \end{bmatrix} \quad (12)$$

Compared with the common state-space representation of the whole power system, $\Delta \mathbf{Z}(t)$ includes the state variables of the i -th FCWG excluding $\Delta \omega_{pr,i}(t)$ and $\Delta x_{p-wt,i}(t)$, as well as all the state variables of other generating units. The dimension of $\Delta \mathbf{Z}(t)$ is $(n-2) \times 1$. Convert (12) from the time domain to frequency domain by the Laplace transform, as given by (13). Similarly, the dimension of $\Delta \mathbf{Z}(s)$ is $(n-2) \times 1$.

$$\begin{bmatrix} s\Delta x_{p-wt,i}(s) \\ s\Delta \omega_{pr,i}(s) \\ s\Delta \mathbf{Z}(s) \end{bmatrix} = \begin{bmatrix} 0 & K_{p-wt,i} & \mathbf{O} \\ A_{21} & 0 & A_{23} \\ A_{31} & A_{32} & A_{33} \end{bmatrix} \begin{bmatrix} \Delta x_{p-wt,i}(s) \\ \Delta \omega_{pr,i}(s) \\ \Delta \mathbf{Z}(s) \end{bmatrix} \quad (13)$$

where $\Delta x_{p-wt,i}(s)$ is the Laplace transform of $\Delta x_{p-wt,i}(t)$; $\Delta \omega_{pr,i}(s)$ is the Laplace transform of $\Delta \omega_{pr,i}(t)$; and $\Delta \mathbf{Z}(s)$ is the Laplace transform of $\Delta \mathbf{Z}(t)$.

Based on (10)–(13), the linearised representation of the whole power system considering the arbitrary control schemes of FCWG in the multi-machine environment can be displayed in Figure 5, where \mathbf{I} is the $(n-2) \times (n-2)$ identity matrix.

From Figure 5, (14)–(16) can be obtained, respectively.

$$\Delta x_{p-wt,i}(s) = \frac{K_{p-wt,i}}{s} \Delta \omega_{pr,i}(s) \quad (14)$$

$$\Delta \omega_{pr,i}(s) = \frac{1}{s} \left(A_{21} \Delta x_{p-wt,i}(s) + A_{23} \Delta \mathbf{Z}(s) \right) \quad (15)$$

$$\Delta \mathbf{Z}(s) = \frac{\mathbf{A}_{31}}{s\mathbf{I} - \mathbf{A}_{33}} \Delta x_{p-wt,i}(s) + \frac{\mathbf{A}_{32}}{s\mathbf{I} - \mathbf{A}_{33}} \Delta \omega_{pr,i}(s) \quad (16)$$

Substitute (14) into (15), and (17) can be obtained.

$$\left(s - A_{21} \frac{K_{p-wt,i}}{s} \right) \Delta \omega_{pr,i}(s) = A_{23} \Delta \mathbf{Z}(s) \quad (17)$$

Substitute (14) into (16), and (18) can be obtained.

$$\Delta \mathbf{Z}(s) = \left(\frac{\mathbf{A}_{31}}{s\mathbf{I} - \mathbf{A}_{33}} \frac{K_{p-wt,i}}{s} + \frac{\mathbf{A}_{32}}{s\mathbf{I} - \mathbf{A}_{33}} \right) \Delta \omega_{pr,i}(s) \quad (18)$$

Substitute (18) into (17), and (19) can be obtained.

$$s = \left(A_{21} + A_{23} \frac{\mathbf{A}_{31}}{s\mathbf{I} - \mathbf{A}_{33}} \right) \frac{K_{p-wt,i}}{s} + \left(A_{23} \frac{\mathbf{A}_{32}}{s\mathbf{I} - \mathbf{A}_{33}} \right) \quad (19)$$

Equation (19) is essentially equivalent to (13). According to Figure 5, (20) can be also derived.

$$\Delta P_{ARC-wt,i}(s) - \Delta P_{we,i}(s) = H_{pr,i} \left(A_{21} \Delta x_{p-wt,i}(s) + A_{23} \Delta \mathbf{Z}(s) \right) \quad (20)$$

Eliminate $\Delta x_{p-wt,i}(s)$ and $\Delta \mathbf{Z}(s)$ in (20) using (14) and (18), and then (21) can be derived.

$$\begin{aligned} & \frac{\Delta P_{ARC-wt,i}(s) - \Delta P_{we,i}(s)}{H_{pr,i} \Delta \omega_{pr,i}(s)} \\ &= \left(A_{21} + A_{23} \frac{\mathbf{A}_{31}}{s\mathbf{I} - \mathbf{A}_{33}} \right) \frac{K_{p-wt,i}}{s} + \left(A_{23} \frac{\mathbf{A}_{32}}{s\mathbf{I} - \mathbf{A}_{33}} \right) \end{aligned} \quad (21)$$

By comparing (19) with (21), it can be seen that (22) can be obtained for an MSO of FCWG.

$$\lambda_d = \frac{\Delta P_{ARC-wt,i}(\lambda_d) - \Delta P_{we,i}(\lambda_d)}{H_{pr,i} \Delta \omega_{pr,i}(\lambda_d)} \quad (22)$$

where λ_d is an eigenvalue of an interested MSO of FCWG.

5 | CONSISTENCY OF MODE SCREENING-BASED EFA TO EIGENVALUE ANALYSIS

In this section, the mode screening-based EFA in Section 3 and the eigenvalue analysis in Section 4 will be proved to be consistent.

Using the Parseval's Theorem, the integral of the product of two real signals can be conducted equivalently in the frequency

domain, as represented by (23).

$$\begin{aligned} \int_{-\infty}^{+\infty} g_1(t)g_2(t)dt &= \frac{1}{2\pi} \int_{-\infty}^{+\infty} G_1(w)G_2^*(w)dw \\ &= \frac{1}{\pi} \int_0^{+\infty} \text{Re} \left(G_1(w)G_2^*(w) \right) dw \end{aligned} \quad (23)$$

where $g_1(t)$ and $g_2(t)$ are two real signals; $G_1(w)$ and $G_2(w)$ are the Fourier transforms of $g_1(t)$ and $g_2(t)$, respectively; and * is the conjugate operator.

Substitute $\Delta P_{ARC-wt,i}(t | \sigma_d)$, $\Delta P_{we,i}(t | \sigma_d)$ and $\Delta \omega_{pr,i}(t | \sigma_d)$ into (23), and then (24) and (25) can be obtained.

$$\begin{aligned} & \int_0^{+\infty} \left(\Delta P_{we,i}(t|\sigma_d) - \Delta P_{ARC-wt,i}(t|\sigma_d) \right) \Delta \omega_{pr,i}(t|\sigma_d) dt \\ &= \frac{1}{\pi} \int_0^{+\infty} \text{Re} \left(\left(\Delta P_{we,i}(w|\sigma_d) - \Delta P_{ARC-wt,i}(w|\sigma_d) \right) \Delta \omega_{pr,i}^*(w|\sigma_d) \right) dw \end{aligned} \quad (24)$$

$$\int_0^{+\infty} \Delta \omega_{pr,i}^2(t|\sigma_d) dt = \frac{1}{\pi} \int_0^{+\infty} \text{Re} \left(\Delta \omega_{pr,i}(w|\sigma_d) \Delta \omega_{pr,i}^*(w|\sigma_d) \right) dw \quad (25)$$

where $\Delta P_{ARC-wt,i}(w | \sigma_d)$, $\Delta P_{we,i}(w | \sigma_d)$ and $\Delta \omega_{pr,i}(w | \sigma_d)$ are the Fourier transforms of $\Delta P_{ARC-wt,i}(t | \sigma_d)$, $\Delta P_{we,i}(t | \sigma_d)$ and $\Delta \omega_{pr,i}(t | \sigma_d)$.

Then, (26) can be derived by applying (24) and (25).

$$\begin{aligned} & \frac{\int_0^{+\infty} \left(\Delta P_{we,i}(t|\sigma_d) - \Delta P_{ARC-wt,i}(t|\sigma_d) \right) \Delta \omega_{pr,i}(t|\sigma_d) dt}{\int_0^{+\infty} \Delta \omega_{pr,i}^2(t|\sigma_d) dt} \\ &= \frac{\int_0^{+\infty} \text{Re} \left(\left(\Delta P_{we,i}(w|\sigma_d) - \Delta P_{ARC-wt,i}(w|\sigma_d) \right) \Delta \omega_{pr,i}^*(w|\sigma_d) \right) dw}{\int_0^{+\infty} \text{Re} \left(\Delta \omega_{pr,i}(w|\sigma_d) \Delta \omega_{pr,i}^*(w|\sigma_d) \right) dw} \end{aligned} \quad (26)$$

For an MSO $\lambda_d = \sigma_d \pm jw_d$, it is noted that $\Delta P_{ARC-wt,i}(w_d | \sigma_d)$, $\Delta P_{we,i}(w_d | \sigma_d)$, $\Delta \omega_{pr,i}(w_d | \sigma_d)$ and $\Delta \omega_{pr,i}^*(w_d | \sigma_d)$ are the constant complex numbers, and the product of $\Delta \omega_{pr,i}(w_d | \sigma_d)$ and $\Delta \omega_{pr,i}^*(w_d | \sigma_d)$ is a real number. Therefore, (9) is further equivalent to (27) on the basis of (26).

$$\begin{aligned} K_{d,i}^{\lambda_d} &= \text{Re} \left(\frac{\left(\Delta P_{we,i}(w_d|\sigma_d) - \Delta P_{ARC-wt,i}(w_d|\sigma_d) \right) \Delta \omega_{pr,i}^*(w_d|\sigma_d)}{\Delta \omega_{pr,i}(w_d|\sigma_d) \Delta \omega_{pr,i}^*(w_d|\sigma_d)} \right) \\ &= \text{Re} \left(\frac{\Delta P_{we,i}(w_d|\sigma_d) - \Delta P_{ARC-wt,i}(w_d|\sigma_d)}{\Delta \omega_{pr,i}(w_d|\sigma_d)} \right) \end{aligned} \quad (27)$$

By comparing (9) with (22) and (27), it can be seen that the proposed damping coefficient in (9) is always equivalent to the

relevant eigenvalue, that is, (28).

$$\text{Re}(\lambda_d) = -\frac{K_{d,i}^{\lambda_d}}{H_{pr,i}} \quad (28)$$

Equation (28) is general for the arbitrary types of control schemes of FCWG, which can be applied for investigating the interested MSOs of FCWG. Then, the application of (28) for estimating the eigenvalue of an interested MSO of FCWG is given as the following steps.

- Step 1: Collect the signals $\Delta P_{ARC-wt,i}(t)$, $\Delta P_{we,i}(t)$ and $\Delta \omega_{pr,i}(t)$ at the i -th PMSG in a period.
- Step 2: Conduct the Fourier transform of $\Delta P_{we,i}(t)$ (or $\Delta \omega_{pr,i}(t)$) to obtain its frequency-amplitude characteristic, from which the angular frequency of dominant MSOs can be observed, i.e., the imaginary parts of eigenvalues of dominant MSOs.
- Step 3: Choose an interested MSO at the angular frequency w_d and give σ_d an initial value as $\sigma_d = 0$.
- Step 4: Calculate $K_{d,i}^{\sigma_d \pm jw_d}$.
- Step 5: If $\text{abs}(-K_{d,i}^{\sigma_d \pm jw_d} / H_{pr,i} - \sigma_d)$ is smaller than an acceptable error e , go to Step 7; otherwise, go to Step 6.
- Step 6: Update σ_d as $\sigma_d = \sigma_d \pm r$ and go to Step 4. It is noted that r/e should be smaller than 10^{-1} .
- Step 7: Output the estimated eigenvalue.

Compared with the traditional eigenvalue analysis, the proposed steps using EFA demonstrate an obvious advantage: only the signal processing is needed, and the complex modelling of the FCWG-penetrated power system can be avoided.

6 | CASE STUDIES

In this section, the mode screening-based EFA is firstly verified in a single-machine infinite-bus (SMIB) power system. Then, the mode screening-based EFA is applied to quantitatively investigated the damping feature of MSOs of FCWG in a 4-machine 2-area (4M2A) power system.

6.1 | Verification of mode screening-based EFA in an SMIB power system

The correctness of (28) is firstly verified in an SMIB power system. The line diagram of this SMIB power system is illustrated in Figure 6. There is an FCWG installed at bus 2 with no ARC. The base capacity of this SMIB power system is 100 MVA. A step-up disturbance happens to PMSG at 0.2 s and its mechanical power becomes 1.1 times of the original value, which lasts for 0.1 s. There is no disturbance on the external grid. In this case study, PMSG and MSC are actually decoupled from the external grid. The parameters of FCWG and traditional synchronous generator are given in the appendix.

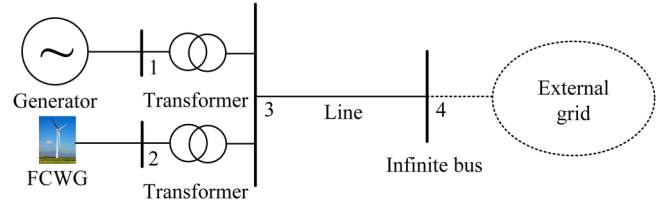


FIGURE 6 Line diagram of an SMIB power system with an FCWG

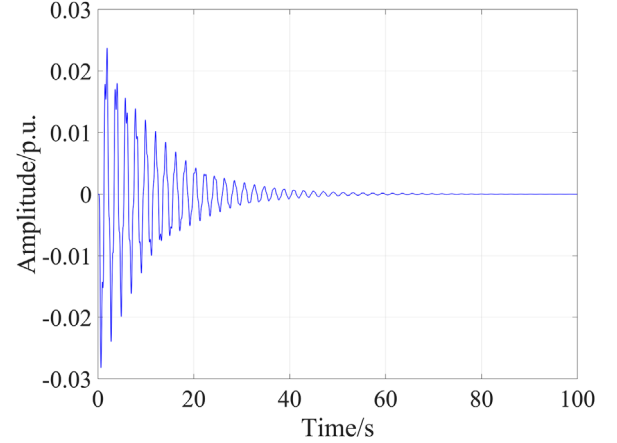


FIGURE 7 The plot of $\Delta P_{we,1}(t)$ in an SMIB power system

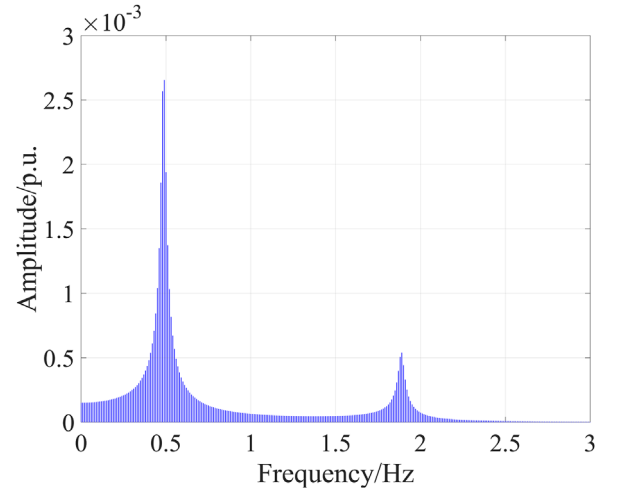


FIGURE 8 The Fourier transform of $\Delta P_{we,1}(t)$ in an SMIB power system

The plot of $\Delta P_{we,1}(t)$ and its amplitude-frequency characteristic are given in Figures 7 and 8. Since the purpose of this case study is to verify the correctness of (28), the eigenvalue of an interested MSO is directly given, that is, $\lambda_d = -0.0883 \pm j3.0530$. Then, the calculation of $-K_{d,1}^{\lambda_d} / H_{pr,1}$ is conducted, and the result is -0.0883 (i.e., $-K_{d,1}^{\lambda_d} / H_{pr,1} = -0.0883$). It can be seen that (28) is valid.

The steps proposed at the end of Section 5 can be feasible, and the estimation of the interested eigenvalue using the proposed steps will be carried out in the next subsection.

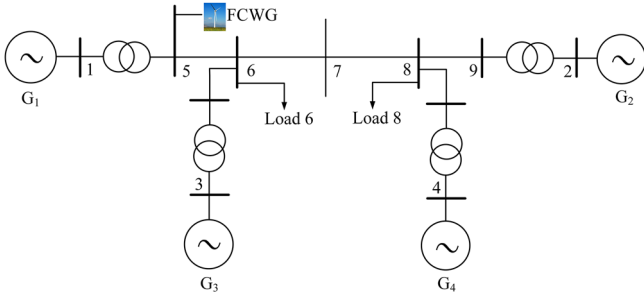


FIGURE 9 Line diagram of a 4M2A power system with an FCWG

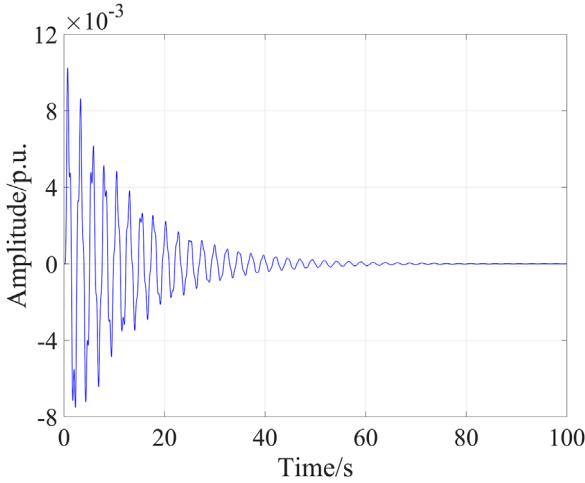


FIGURE 10 The plot of $\Delta P_{we,1}(t)$ in Scenario 1 of a 4M2A power system

6.2 | Application of mode screening-based EFA in a 4M2A power system

The line diagram of a 4M2A power system is given by Figure 9. There is an FCWG installed at bus 5 with the integration of an ARC. The base capacity of this power system is 100 MVA. The parameters of FCWG and traditional synchronous generators are given in the appendix.

6.2.1 | Scenario 1 (machine-side disturbance)

In Scenario 1, there is no disturbance on the external power grid, but a disturbance occurs to the mechanical power of PMSG at 0.2 s and its value becomes 1.05 of the original one, which lasts for 0.1 s.

The plot of $\Delta P_{we,1}(t)$ is given in Figure 10, and the Fourier transform of $\Delta P_{we,1}(t)$ is given in Figure 11. It can be seen that there are two inherent MSOs excited at 0.41 Hz and 1.54 Hz, which are selected as the interested ones. The imaginary parts of the interested eigenvalues are estimated as $2\pi \times 0.41j = 2.5761j$ and $2\pi \times 1.54j = 9.6761j$.

According to the mentioned Steps 1–7 at the end of Section 5, the real parts of eigenvalues of the inherent MSOs at around 0.41 Hz and 1.54 Hz are estimated. The results are listed in Table 1. It is noted that the real eigenvalues are calculated

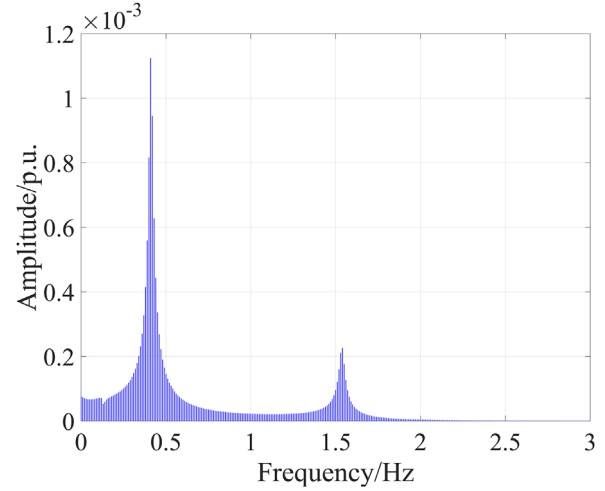


FIGURE 11 The Fourier transform of $\Delta P_{we,1}(t)$ in Scenario 1 of a 4M2A power system

TABLE 1 Application of EFA for estimating interested eigenvalues in Scenario 1 of a 4M2A power system

Interested frequency	Real eigenvalue	Estimated eigenvalue
0.41 Hz (inherent)	$-0.0761 \pm 2.5889j$	$-0.0761 \pm 2.5761j$
1.54 Hz (inherent)	$-0.0997 \pm 9.6595j$	$-0.0998 \pm 9.6761j$

from the state matrix, which acts as a comparison. It can be found that the numerical estimation from the proposed Steps 1–7 has a high accuracy.

Through the study in Scenario 1, it can be revealed that the machine-side disturbances such as continuous wind fluctuations will only trigger the inherent MSOs, and the non-inherent MSO will not be excited even if the ARC is installed. The damping feature of the inherent MSOs of FCWG can be evaluated accurately by the mode screening-based EFA proposed in this paper.

6.2.2 | Scenario 2 (grid-side disturbance)

In Scenario 2, there is no disturbance on the machine side of FCWG originally. A disturbance occurs to the mechanical power of G_1 (i.e., a traditional synchronous generator in this 4M2A power system) at 0.2 s and its value becomes 1.05 of the original one, which lasts for 0.1 s.

The plots of $\Delta P_{we,1}(t)$ and $\Delta P_{ARC-wt,1}(t)$ are given in Figures 12 and 14, and the Fourier transform of $\Delta P_{we,1}(t)$ and $\Delta P_{ARC-wt,1}(t)$ are given in Figures 13 and 15. It can be seen from Figure 13 that there are three dominant MSOs at 0.41 Hz, 0.53 Hz, and 1.54 Hz monitored on the machine side of FCWG. It is known from Figure 15 that the non-inherent MSO of 0.53 Hz is actually the inter-area oscillation mode of the external power grid that is introduced by ARC to the machine side of FCWG. While the MSOs of 0.41 Hz and 1.54 Hz are the inherent ones of FCWG that are excited by the ARC. The imaginary

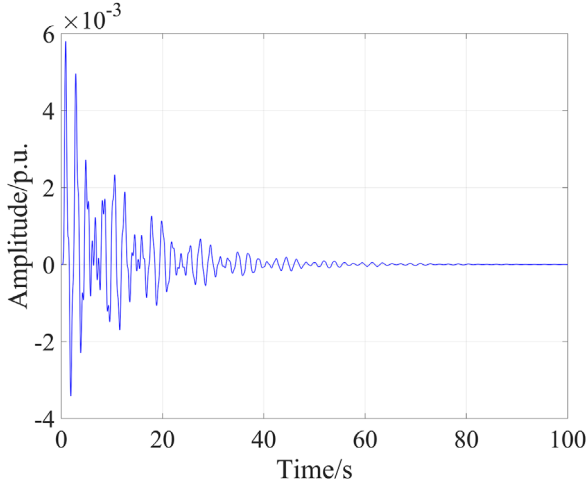


FIGURE 12 The plot of $\Delta P_{we,1}(t)$ in Scenario 2 of a 4M2A power system

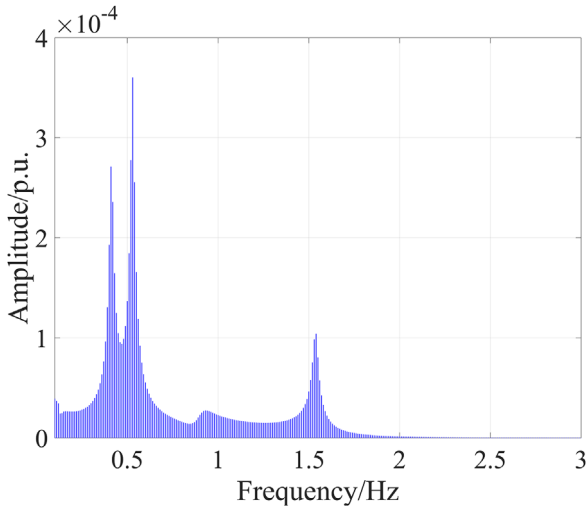


FIGURE 13 The Fourier transform of $\Delta P_{we,1}(t)$ in Scenario 2 of a 4M2A power system

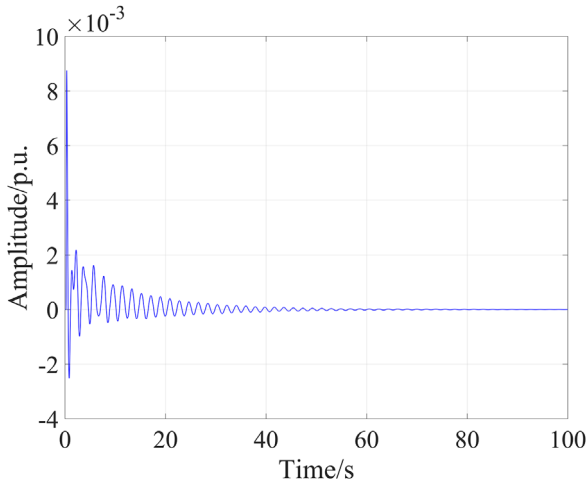


FIGURE 14 The plot of $\Delta P_{ARC-w,1}(t)$ in Scenario 2 of a 4M2A power system

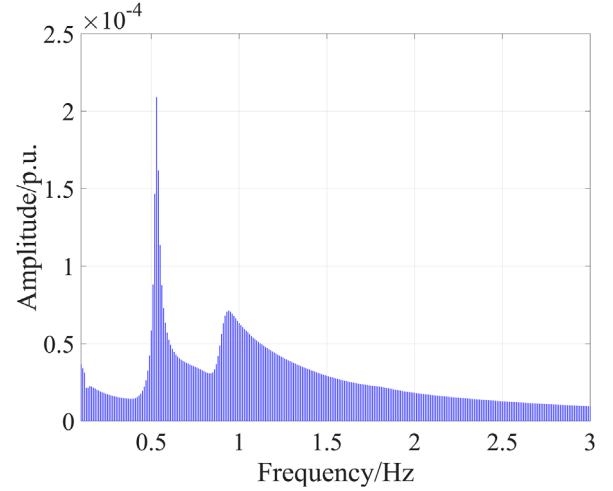


FIGURE 15 The Fourier transform of $\Delta P_{ARC-w,1}(t)$ in Scenario 2 of a 4M2A power system

TABLE 2 Application of EFA for estimating interested eigenvalues in Scenario 2 of a 4M2A power system

Interested frequency	Real eigenvalue	Estimated eigenvalue
0.41 Hz (inherent)	$-0.0761 \pm 2.5889j$	$-0.0760 \pm 2.5761j$
0.53 Hz (non-inherent)	$-0.0682 \pm 3.3264j$	$-0.0682 \pm 3.3301j$
1.54 Hz (inherent)	$-0.0997 \pm 9.6595j$	$-0.0998 \pm 9.6761j$

part of the eigenvalue of the non-inherent MSO is estimated as $2\pi \times 0.53j = 3.3301j$.

According to the mentioned Steps 1–7 at the end of Section 5, the real parts of interested eigenvalues are estimated. The results are listed in Table 2. It can be found that the numerical estimations from the proposed Steps 1–7 demonstrate a high accuracy in Scenario 2.

Through the study in Scenario 2, it can be seen that the grid-side disturbances can be propagated to the machine side through ARC and excite the inherent MSOs of FCWG. The non-inherent MSO of FCWG can be only triggered by the grid-side disturbances and introduced by ARC to the machine side of FCWG. The damping feature of both types of MSOs can be assessed by the mode screening-based EFA proposed in this paper.

6.2.3 | Scenario 3 (machine and grid-side disturbances)

In Scenario 3, a three-phase short-circuit fault occurs to the external power grid at 0.2 s, which lasts for 0.1 s. Meanwhile, a continuous disturbance happens to the mechanical power of PMSG.

The plot of $\Delta P_{we,1}(t)$ and its Fourier transform are given in Figures 16 and 17. It can be seen that the three-phase short-circuit fault of the external power grid can bring a great risk to the machine side dynamics of FCWG through ARC.

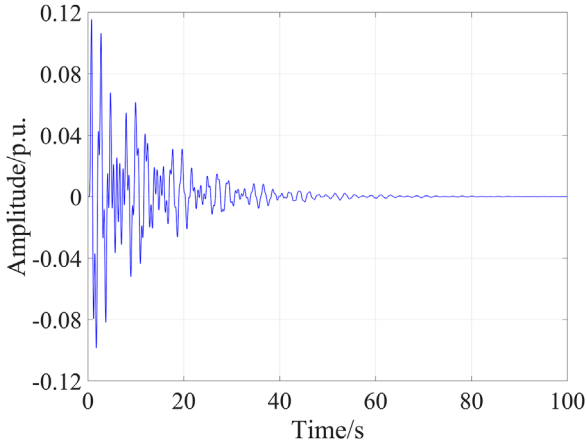


FIGURE 16 The plot of $\Delta P_{we,1}(t)$ in Scenario 3 of a 4M2A power system

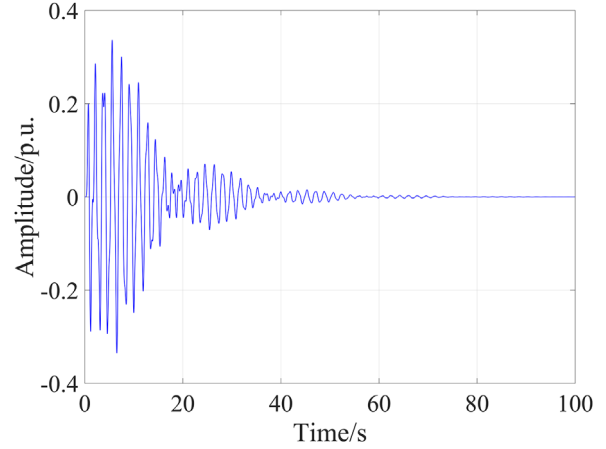


FIGURE 18 The plot of $\Delta P_{we,1}(t)$ in Scenario 4 of a 4M2A power system

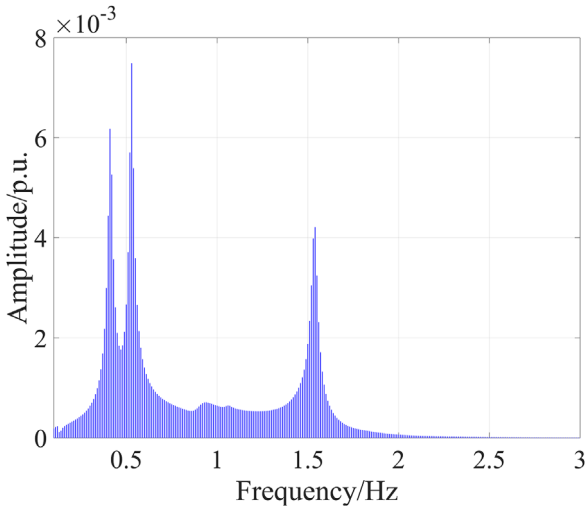


FIGURE 17 The Fourier transform of $\Delta P_{we,1}(t)$ in Scenario 3 of a 4M2A power system

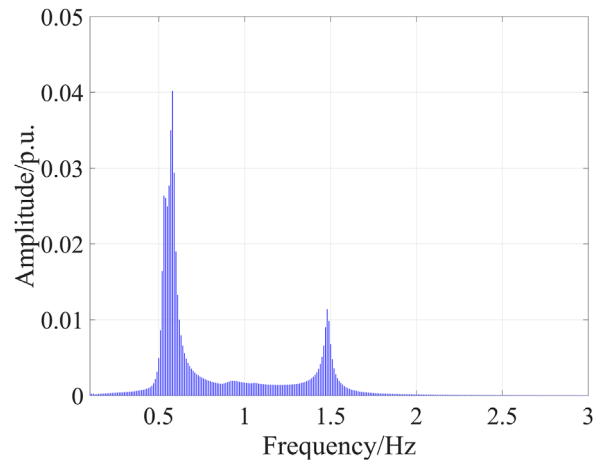


FIGURE 19 The Fourier transform of $\Delta P_{we,1}(t)$ in Scenario 4 of a 4M2A power system

TABLE 3 Application of EFA for estimating interested eigenvalues in Scenario 3 of a 4M2A power system

Interested frequency	Real eigenvalue	Estimated eigenvalue
0.41 Hz (inherent)	$-0.0761 \pm 2.5889j$	$-0.0761 \pm 2.5761j$
0.53 Hz (non-inherent)	$-0.0682 \pm 3.3264j$	$-0.0681 \pm 3.3301j$
1.54 Hz (inherent)	$-0.0997 \pm 9.6595j$	$-0.0998 \pm 9.6761j$

The real parts of eigenvalues of the interested MSOs are estimated, and the results are listed in Table 3, which still shows a high accurate.

Through the study in Scenario 3, it can be indicated that the superposition of grid-side short-circuit fault and machine-side disturbance of FCWG can pose a great threat to machine-side dynamics of FCWG. Both disturbances would contribute to the amplitude of the inherent MSOs. The proposed EFA still possesses a high accuracy in this case.

6.2.4 | Scenario 4 (modal resonance)

In Scenario 4, the setting of the machine and grid-side disturbances is same with that in Scenario 3, but the setting of parameters of MSC is different from those in Scenario 3. The frequency of the inherent MSO becomes closer to that of the non-inherent MSO in this scenario.

The plot of $\Delta P_{we,1}(t)$ and its Fourier transform are given in Figures 18 and 19. It can be seen that the amplitudes at 0.53 Hz and 0.58 Hz are much larger than the two in Scenario 3. There are three dominant MSOs at 0.53 Hz, 0.58 Hz and 1.48 Hz. Among them, the MSO of 0.53 Hz is the non-inherent one introduced by ARC, and the MSOs of 0.58 Hz and 1.48 Hz are the inherent ones. The real eigenvalues and estimated eigenvalues are list in Table 4.

Through the study in Scenario 4, it can be concluded that the improper parameter settings of controllers can cause the modal resonance between the inherent and non-inherent MSOs of FCWG. The proposed EFA can accurately estimate the damping feature of MSOs to reduce this potential risk.

TABLE 4 Application of EFA for estimating interested eigenvalues in Scenario 4 of a 4M2A power system

Interested frequency	Real eigenvalue	Estimated eigenvalue
0.53 Hz (non-inherent)	$-0.0751 \pm 3.3227j$	$-0.0752 \pm 3.3301j$
0.58 Hz (inherent)	$-0.0799 \pm 3.6447j$	$-0.0799 \pm 3.6442j$
1.48 Hz (inherent)	$-0.0889 \pm 9.3138j$	$-0.0890 \pm 9.2991j$

7 | CONCLUSION

In this paper, a mode screening-based EFA is proposed and conducted for MSOs of FCWG, and its consistency with the eigenvalue analysis is strictly revealed considering the arbitrary control schemes of FCWG in the multi-machine environment. On this basis, the proposed EFA is applied to investigate the damping feature of multiple types of MSOs of FCWG in different scenarios through the case studies of the SMIB and 4M2A power systems.

The key findings of the paper are listed as follows: (i) the inherent MSO of FCWG can be excited by the machine-side disturbances, while the non-inherent MSO would not be excited by the machine-side disturbances regardless of the installation of ARC. The damping feature of inherent MSOs of FCWG can be accurately investigated by the proposed EFA accurately and efficiently; (ii) when ARC is used, the grid-side oscillation mode excited by the grid-side disturbances can be introduced to the machine side of FCWG and becomes the non-inherent MSO. The inherent MSOs of FCWG can also be excited by the propagation of grid-side disturbances through ARC. The proposed EFA can perform satisfactorily in obtaining the damping feature of both the inherent and non-inherent MSO introduced by ARC; (iii) the superposition of grid-side short-circuit fault and machine-side disturbance of FCWG can significantly deteriorate the machine-side dynamic performance of FCWG especially for inherent MSOs in terms of the oscillatory amplitude, and the accuracy of the estimated damping feature of MSOs can be also guaranteed under more severe disturbance condition; and (iv) when the frequency of the inherent MSO is closer to that of the non-inherent MSO introduced by ARC, the severe modal resonance can be triggered on the machine side of FCWG, and the accuracy of the proposed EFA can be still ensured under this resonance condition.

ACKNOWLEDGEMENTS

The authors would like to thank the National Natural Science Foundation of China for the Research Project (51807171), the Guangdong Science and Technology Department for the Research Project (2019A1515011226), the Hong Kong Research Grant Council for the Research Projects (15200418) and (15219619), and the Department of Electrical Engineering, The Hong Kong Polytechnic University for the Start-up Fund Research Project (1-ZE68).

CONFLICT OF INTEREST

There is no conflict of interest.

DATA AVAILABILITY STATEMENT

The data that support the findings of this study are available from the corresponding author upon reasonable request.

ORCID

Yong Hu  <https://orcid.org/0000-0002-3776-3103>

Siqi Bu  <https://orcid.org/0000-0002-1047-2568>

Jianqiang Luo  <https://orcid.org/0000-0003-0537-0572>

REFERENCES

- Li, J., Wang, S., Ye, L. et al.: A coordinated dispatch method with pumped-storage and battery-storage for compensating the variation of wind power. *Prot. Control Mod. Power Syst.* 3, 1–14 (2018)
- Badal, F. R., Das, P., Sarker, S. K., et al.: A survey on control issues in renewable energy integration and microgrid. *Prot. Control Mod. Power Syst.* 4, 1–27 (2019)
- Luo, J., Bu, S., Zhu, J., et al.: Modal shift evaluation and optimization for resonance mechanism investigation and mitigation of power systems integrated with FCWG. *IEEE Trans. Power Syst.* 35(5), 4046–4055 (2020)
- Liu, H., Xie, X., He, J., et al.: Subsynchronous interaction between direct-drive PMSG based wind farms and weak AC networks. *IEEE Trans. Power Syst.* 32(6), 4708–4720 (2017)
- Luo, J., Bu, S., Teng, F.: An optimal modal coordination strategy based on modal superposition theory to mitigate low frequency oscillation in FCWG penetrated power systems. *Int. J. Electr. Power Energy Syst.* 120, 105975 (2020)
- Feng, S., Wang, K., Lei, J., et al.: Influences of DC bus voltage dynamics in modulation algorithm on power oscillations in PMSG-based wind farms. *Int. J. Electr. Power Energy Syst.* 124, 106387 (2021)
- Luo, J., Zou, Y., Bu, S., et al.: Converter-driven stability analysis of power systems integrated with hybrid renewable energy sources. *Energies* 14(14), 1–20 (2021)
- Luo, J., Bu, S., Chung, C. Y.: Design and comparison of auxiliary resonance controllers for mitigating modal resonance of power systems integrated with wind generation. *IEEE Trans. Power Syst.* 36(4), 3372–3383 (2021)
- Gao, F., Zheng, X., Bozhko, S., et al.: Modal analysis of a PMSG-based DC electrical power system in the more electric aircraft using eigenvalues sensitivity. *IEEE Trans. Transp. Electr.* 1(1), 65–76 (2015)
- Xia, S. W., Bu, S. Q., Zhang, X., et al.: Model reduction strategy of doubly-fed induction generator-based wind farms for power system small-signal rotor angle stability analysis. *Appl. Energy* 222, 608–620 (2018)
- Chen, L., Xu, F., Min, Y., et al.: Transient energy dissipation of resistances and its effect on power system damping. *Int. J. Electr. Power Energy Syst.* 91, 201–208 (2017)
- Luo, J., Bu, S., Zhu, J.: A novel PMU-based adaptive coordination strategy to mitigate modal resonance between full converter-based wind generation and grids. *IEEE J. Emerging Sel. Top. Power Electron.* 9(6), 7173–7182 (2021)
- Meegahapola, L. G., Bu, S., Wadduwage, D. P., et al.: Review on oscillatory stability in power grids with renewable energy sources: Monitoring, analysis, and control using synchrophasor technology. *IEEE Trans. Ind. Electron.* 68(1), 519–531 (2021)
- Shu, Y., Zhou, X., Li, W.: Analysis of low frequency oscillation and source location in power systems. *CSEE J. Power Energy Syst.* 4(1), 58–66 (2018)
- Chen, L., Min, Y., Hu, W.: An energy-based method for location of power system oscillation source. *IEEE Trans. Power Syst.* 28(2), 828–836 (2013)
- Chen, L., Min, Y., Lu, X., et al.: Online emergency control to suppress frequency oscillations based on damping evaluation using dissipation energy flow. *Int. J. Electr. Power Energy Syst.* 103, 414–420 (2018)
- Xie, R., Trudnowski, D. J.: Tracking the damping contribution of a power system component under ambient conditions. *IEEE Trans. Power Syst.* 33(1), 1116–1117 (2018)
- Maslennikov, S., Wang, B., Litvinov, E.: Dissipating energy flow method for locating the source of sustained oscillations. *Int. J. Electr. Power Energy Syst.* 88, 55–62 (2017)

19. Chen, L., Min, Y., Chen, Y.-P., et al.: Evaluation of generator damping using oscillation energy dissipation and the connection with modal analysis. *IEEE Trans. Power Syst.* 29(3), 1393–1402 (2014)
20. Hu, Y., Bu, S., Zhou, B., et al.: Impedance-based oscillatory stability analysis of high power electronics-penetrated power systems—A survey. *IEEE Access* 7, 120774–120787 (2019)
21. Karaagac, U., Mahseredjian, J., Gagnon, R., et al.: A generic EMT-type model for wind parks with permanent magnet synchronous generator full size converter wind turbines. *IEEE Power Energy Technol. Syst. J.* 6(3), 131–141, (2019)
22. Kundur, P., Balu, N. J., Lauby, M. G.: *Power System Stability and Control*. McGraw-Hill, New York (1994)

How to cite this article: Hu, Y., Bu, S., Luo, J.: Application of energy flow analysis in investigating machine-side oscillations of full converter-based wind generation systems. *IET Renew. Power Gener.* 16, 900–911 (2022). <https://doi.org/10.1049/rpg2.12387>

APPENDIX A

Parameters in an SMIB power system

The parameters of PMSG are as follows [8]:

$$P_{pm,1} = 1.0 \text{ p.u.}; H_{pr,1} = 8.0 \text{ s}; X_{pd,1} = 0.2 \text{ p.u.};$$

$$X_{pq,1} = 0.2 \text{ p.u.}; X_{pf,1} = 0.02 \text{ p.u.}$$

where $X_{pd,1}$ is the d -axis reactance of the stator winding; $X_{pq,1}$ is the q -axis reactance of the stator winding; and $X_{pf,1}$ is the filter reactance.

The parameters of MSC are as follows:

$$K_{pp-wt,1} = 1.25; K_{p-wt,1} = 70.0; K_{pp-iq,1} = 0.08; K_{p-iq,1} = 30.0;$$

$$K_{pp-id,1} = 1.01; K_{p-id,1} = 10.0$$

The parameters of the traditional synchronous generator are as follows [22]:

$$T_j = 8.0 \text{ s}; D = 0; \omega_0 = 314.0 \text{ rad/s}; T'_{d0} = 5.0 \text{ s};$$

$$X_d = 0.8 \text{ p.u.}; X_q = 0.4 \text{ p.u.}; X'_d = 0.05 \text{ p.u.}; P_{m0} = 0.6 \text{ p.u.}$$

where T_j denotes the inertia constant; D denotes the natural damping; ω_0 denotes the synchronous angular frequency; T'_{d0}

denotes the time constant of the field winding; X_d is the d -axis synchronous reactance; X_q is the q -axis synchronous reactance; X'_d is the d -axis transient reactance; and P_{m0} denotes the initial mechanical power.

Parameters in a 4M2A power system

The parameters of PMSG are as follows [8]:

$$P_{pm,1} = 1.0 \text{ p.u.}; H_{pr,1} = 8.0 \text{ s}; X_{pd,1} = 0.2 \text{ p.u.};$$

$$X_{pq,1} = 0.2 \text{ p.u.}; X_{pf,1} = 0.02 \text{ p.u.}$$

The parameters of MSC in Scenarios 1–3 are as follows:

$$K_{pp-wt,1} = 1.05; K_{p-wt,1} = 50.0; K_{pp-iq,1} = 0.07; K_{p-iq,1} = 20.0;$$

$$K_{pp-id,1} = 0.04; K_{p-id,1} = 30.0$$

The parameters of MSC in Scenario 4 are as follows:

$$K_{pp-wt,1} = 1.05; K_{p-wt,1} = 92.0; K_{pp-iq,1} = 0.07; K_{p-iq,1} = 20.0;$$

$$K_{pp-id,1} = 0.04; K_{p-id,1} = 30.0$$

The parameters of ARC are as follows:

$$T_1 = 0.3 \text{ s}; T_2 = 0.03 \text{ s}; T_3 = 0.3 \text{ s}; T_4 = 0.03 \text{ s};$$

$$T_W = 0.05 \text{ s}; K_W = 0.8$$

The parameters of traditional synchronous generators are as follows [22]:

$$T_{j,1} = T_{j,2} = 117.0 \text{ s}; T_{j,3} = T_{j,4} = 111.15 \text{ s};$$

$$D_1 = D_2 = D_3 = D_4 = 0;$$

$$\omega_0 = 314.0 \text{ rad/s}; T'_{d0,1} = T'_{d0,2} = T'_{d0,3} = T'_{d0,4} = 8.0 \text{ s};$$

$$X_{d,1} = X_{d,2} = X_{d,3} = X_{d,4} = 0.2 \text{ p.u.}; X_{q,1} = X_{q,2}$$

$$= X_{q,3} = X_{q,4} = 0.1889 \text{ p.u.};$$

$$X'_{d,1} = X'_{d,2} = X'_{d,3} = X'_{d,4} = 0.0333 \text{ p.u.}; P_{m0,1} = 6.0 \text{ p.u.};$$

$$P_{m0,3} = 7.5 \text{ p.u.}; P_{m0,2} = P_{m0,4} = 7.0 \text{ p.u.}$$